Evolution of a Triad Twisted String Actuator for Controlling a Two Degrees of Freedom Joint to Improve Performance and Allow for Active Transmission Adjustment

Damian Crosby, Joaquin Carrasco *Member, IEEE*, William Heath *Member, IEEE*, and Andrew Weightman

***Abstract*—Actuated universal joints are used in a wide range of robotic applications, including mobile snake robots, snake-arm robots and robotic tails. Depending on the application and design constraints, these can use remote cable or fluid driven systems, or inline motors. In order to realise the benefits of inline actuation while keeping the system compact with a high power to weight ratio, an actuated universal joint (AUJ) was developed using an "antagonistic triad" of three twisted string actuators. However, the design of this system had numerous drawbacks in its prototype form, namely a limited angle range, poor accuracy due to the angular feedback sensors used, and issues with string failure due to mechanical design choices. In this publication, these challenges are addressed through design changes, and angle range was increased from $\pm 14.5^\circ$ to $\pm 26^\circ$ for a single axis, and $\pm 6^\circ$ to $\pm 20^\circ$ for a dual axis movement.**

***Index Terms*—Flexible Robots, Force Control, Tendon/Wire Mechanism, Twisted String Actuator.**

I. Introduction

ACTUATED universal joint (AUJ) mechanisms are found in a wide range of robotic applications that require soft-rigid reconfigurable mechanisms, such as confined space inspection using continuum robots [1], highly manoeuvrable mobile snake robots [2], and biomimetic robot tails for stability [3]. These can either use inline actuators which directly move the joint [4]–[6], or cable/fluid driven systems that rely on a static "base" to house the actuators or compressors [7]. In the former case, this results in high torque requirements for the actuators, as they have to lift the mass of all the actuators in subsequent sections. In the latter case, space is required for the base, which is not practical in all applications, such as mobile robots.

D. Crosby, and A. Weightman are with the Department of Mechanical, Aerospace and Civil Engineering, School of Engineering, Faculty of Science and Engineering, The University of Manchester, Manchester, United Kingdom.

J. Carrasco and W. Heath are with the Department of Electrical and Electronic Engineering, School of Engineering, Faculty of Science and Engineering, The University of Manchester, Manchester, United Kingdom.

First developed by Würtz *et al.* [8] in 2010, the twisted string actuator (TSA) uses two or more strings between two fixtures as a linear actuator. When one fixture is rotated (typically by an electric motor), the looped string twists into a helix, decreasing the distance between them. Given the unwound length l_u, and the cross-section radius of the string r_s (or $r_s + r_c$ when there are more than two strings, where r_c is the radius of a tangentially constrained circle drawn between the strings), the actuator length is given by

$$l_s(\theta_s) = \sqrt{l_u^2 - \theta_s^2 r_s^2} \tag{1}$$

where θ_s is the motor angle in radians. TSA actuators have been used for a hand orthosis [9], elbow joint [10] and foldable robot arm [11] among other functions.

Whereas alternative electric actuation systems, such as leadscrews, require the addition of gearing for significant increases in reduction (lower velocity, higher torque), which increases actuator size and mass, a TSA can increase reduction by reducing string thickness or string count, which slightly reduces actuator mass [12]. In the case of leadscrews, the reduction can be increased marginally by decreasing thread lead [13], but this can quickly come up against manufacturing tolerances and material stiffness and toughness limitations. The screw radius can also be increased, but this has the effect of increasing actuator size and mass in a similar fashion.

One of the main challenges of TSA is the reduction changes depending on the motor angle (and therefore actuator position). This is an inverse nonlinear relationship, where the function has a decreasing derivative as the motor angle increases [8], [12]. String compliance may also need to be considered under high force conditions, but this can be mitigated with accurate modelling [14], or a suitably robust control strategy that can ignore compliance in its system model [8], [12]. Since strings are not rigid, TSA can only impart force in tension, and 1 degree of freedom (DOF) single TSA actuator joints must make use of a spring return mechanism [15]–[17], which can limit actuator range since the spring force increases as maximum TSA force decreases [18]. Usman *et al.* [18] developed a linear force return mechanism ($k = 0$) to partially mitigate this issue, but an ideal situation is to have a matching antagonistic force profile. This can be done by using a second TSA actuator which is synchronised with the first [10], [19]–[21]. Therefore, by adding a third TSA, a 2 DOF actuator can be realised without the use of springs.

The use of TSA as an actuator for an AUJ is an understudied area of research. Konda, Bombara, Chow, *et al.* [22] have proposed a similar design using a flexible core with continuous curvature as opposed to a rigid universal joint, which outlines an open loop control solution for multi axis control using only two TSA experimentally demonstrated with a limited azimuthal axis range in polar coordinates. For the first time the authors demonstrate a robust closed loop control of an AUJ in both axes of motion, including the full azimuthal range of $[0, 360)\,°$, using three TSA in an "antagonistic triad" configuration. The result is a light, compact AUJ design that has the potential to significantly improve upon exiting inline actuation options.

In this publication, the authors aim to improve on the prototype constructed in [23], previously published as a conference proceeding at the IEEE International Conference on Robotics and Automation (ICRA) 2022, by demonstrating performance improvements in joint angle range, string lifetime, and investigating the use of active transmission adjustment (ATA), for adjustments to the dynamics of the system in real time. The results of investigations into increased follower mass and joint velocity are also presented, an evolution from our original conference procceding [23].

A. Design Summary

Because TSA can can only operate in tension, a minumum of three TSA are required to operate an AUJ. These can be arranged into an "Antagontic Triad" where adjusting the length of each TSA changes the orientation of the AUJ, in a similar fashion to other cable driven robotic systems [7]. These lengths can be combined into a vector function $\Lambda(\boldsymbol{\theta}) = \begin{bmatrix}\lambda_1(\boldsymbol{\theta}) & \lambda_2(\boldsymbol{\theta}) & \lambda_3(\boldsymbol{\theta})\end{bmatrix}$ where

$$\begin{aligned}\lambda_1(\boldsymbol{\theta}) &= \sqrt{\begin{aligned}&a + 2l_1 r \sin(\theta_2)\cos(\theta_1) + l_2^2 \\ &\quad + 2l_2 r \sin(\theta_2) - 2r^2\cos(\theta_2) + 2r^2\end{aligned}} \\ \lambda_2(\boldsymbol{\theta}) &= \sqrt{a+b+c-d} \\ \lambda_3(\boldsymbol{\theta}) &= \sqrt{a-b-c+d}\end{aligned}$$

where:

$$\begin{aligned}a &= l_1^2 + 2l_1 l_2 \cos(\theta_1)\cos(\theta_2) \\ b &= \sqrt{3}l_1 r \sin(\theta_1) - l_1 r \sin(\theta_2)\cos(\theta_1) + l_2^2 \\ c &= \sqrt{3}l_2 r \sin(\theta_1)\cos(\theta_2) - l_2 r \sin(\theta_2) \\ d &= \frac{\sqrt{3}r^2\sin(\theta_1)\sin(\theta_2)}{2} - \frac{3r^2\cos(\theta_1)}{2} - \frac{r^2\cos(\theta_2)}{2} + 2r^2.\end{aligned} \tag{2}$$

where $\Lambda(\boldsymbol{\theta}) = \begin{bmatrix}\lambda_1(\boldsymbol{\theta}) & \lambda_2(\boldsymbol{\theta}) & \lambda_3(\boldsymbol{\theta})\end{bmatrix}$ is a vector function which outputs the magnitudes of each point pair, and therefore the lengths of each actuator, assuming both ends of each actuator can rotate freely on both x and y axes. Figure 1 is a kinematic diagram of the antagonistic triad.

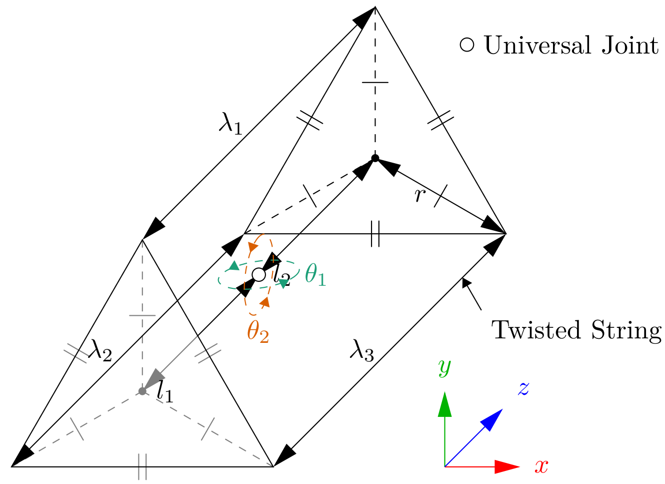

Fig. 1: Kinematic diagram of the antagonistic triad, where the universal joint rotation is defined by $\theta_{1,2}$ on the y and x axes respectively, and the actuator lengths are defined by $\lambda_{1,2,3}$ for the *top*, *left* and *right* strings. r and $l_{1,2}$ define the anchor points of the strings.

After an investigation into a position based kinematic control system in the original design proved unsuccessful, a force based control system was developed, which uses the inverse dynamics of the AUJ to convert angular velocity from a PID controller into angular torque, which is then turned into force setpoints for each TSA using an optimising algorithm based on [24]. The control system is a four layer cascade design, joining an outer loop PID controller C_1 to an inverse dynamic control system C_2 [25], to the triad force controller C_3 in [24], to a proportional controller C_4 for each TSA. It uses feedback signals of the joint position and TSA force.

C_3 uses the *inverse force transformation* algorithm from [24] with the jacobian in (2) to select an optimal force vector from the desired joint torque. Here it is presented in an unexpanded and more general form,

$$\begin{aligned}J_\Lambda &= \begin{bmatrix}\frac{\partial\lambda_1}{\partial\theta_1} & \frac{\partial\lambda_2}{\partial\theta_1} & \frac{\partial\lambda_3}{\partial\theta_1} \\ \frac{\partial\lambda_1}{\partial\theta_2} & \frac{\partial\lambda_2}{\partial\theta_2} & \frac{\partial\lambda_3}{\partial\theta_2}\end{bmatrix} \\ \boldsymbol{\gamma}(i) &= -J_{\Lambda_{-i,*}}^{-\intercal}\left(J_{\Lambda_{i,*}}^{\intercal} f_{\min} + \boldsymbol{\tau}\right) \\ \boldsymbol{F}(\boldsymbol{\tau},\boldsymbol{\theta}) &= \begin{bmatrix}f_{\min} & \boldsymbol{\gamma}(2)_1 & \boldsymbol{\gamma}(3)_1 \\ \boldsymbol{\gamma}(1)_1 & f_{\min} & \boldsymbol{\gamma}(3)_2 \\ \boldsymbol{\gamma}(1)_2 & \boldsymbol{\gamma}(2)_2 & f_{\min}\end{bmatrix}.\end{aligned} \tag{3}$$

A force matrix F is created from the torque input $\boldsymbol{\tau}$, jacobian J_Λ from the vector function Λ as defined in equation 2, and minimum force constant f_{min}. f_{ii} is equal to f_{min}, while the other elements in the column are based on a calculation using $J_{\Lambda_{-i,*}}$ where $-i$ is a row removed from the matrix. Algorithm 1 is then used to create output force vector $\boldsymbol{f}$, which minimises the net force on all TSA while producing the desired output torque on the universal joint.

Figure 2 shows a complete block diagram of the control system.

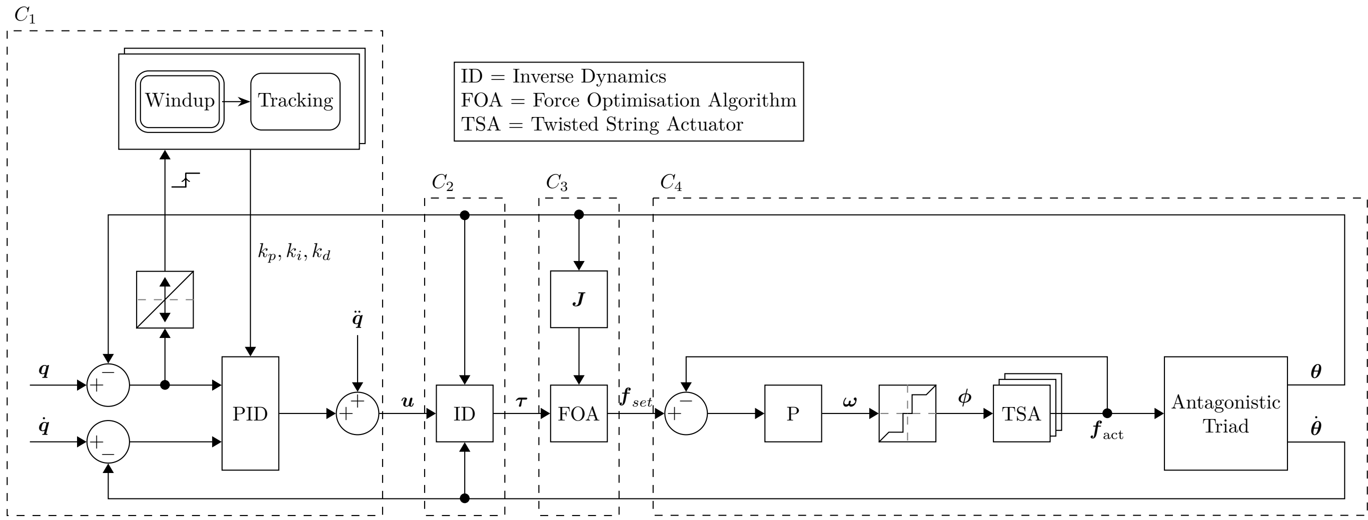

Fig. 2: Block diagram of the complete experimental control system, excluding the hardware velocity controllers for the motors. Dashed boxes correspond to the control layers $C_{1\ldots4}$.

Algorithm 1 Selects one column of $\boldsymbol{F}$ to be the output force vector $\boldsymbol{f}$, where $\top$ and $\bot$ are boolean *true* and *false* respectively, and $\boldsymbol{f}_{*,i}$ is the ith column of F.

$\boldsymbol{s} \leftarrow \begin{bmatrix} \top & \top & \top \end{bmatrix}$
if $f_{23} > f_{\min}$ **then** $s_2 \leftarrow \bot$ **else** $s_3 \leftarrow \bot$ **end if**
if $f_{31} > f_{\min}$ **then** $s_3 \leftarrow \bot$ **else** $s_1 \leftarrow \bot$ **end if**
if $f_{12} \geq f_{\min}$ **then** $s_1 \leftarrow \bot$ **else** $s_2 \leftarrow \bot$ **end if**
for $i = 1$ to 3 **do**
    if $s_i \rightarrow \top$ **then** $\boldsymbol{f}_{\text{set}} \leftarrow \boldsymbol{f}_{*,i}$ **end if**
end for

II. Improvements to Original Design

A. Increasing AUJ Angle Range

The AUJ angle tracking experiments in [23] only had a range of $\pm 14.5°$ in a single axis, and $\pm 6°$ for both axes. This was because one or more TSA would completely "unwind" near that limit and be unable to lengthen further. This limits the practicality of such a mechanism, for example a multi-segment design would have a very large minimum curvature. Increasing $f_{\min}$ does increase the angle range marginally by increasing the TSA motor angle at $\boldsymbol{\theta} = \begin{bmatrix} 0 & 0 \end{bmatrix}^\intercal$, which was proven experimentally. These experiments were able to achieve modest increases of $4.004\,°\,\mathrm{N}^{-1}$ for the positive (upper) limit of the universal joint roll θ_1, and $-6.062\,°\,\mathrm{N}^{-1}$ for the negative (lower) limit, within the $f_{\min}$ interval $[3, 3.5]$. However, further attempts to increase $f_{\min}$, or attempts to perform the same experiment on the pitch axis resulted in premature string failure. It was also clear to achieve significant increases in AUJ angle range, a different approach would be needed that would require modifications to the design.

The most effective modification to improve AUJ angle range is to reduce the value of r in (2). This decreases the stroke length required for each TSA to achieve the same AUJ angle range as shown by table I, which also reduces the TSA motor angle accordingly, allowing a greater AUJ angle to be reached before one or more TSA unwind. This can be done by using smaller motors, or by using the same size or larger motors with offset shafts connected by spur gears. Smaller motors were chosen, with a cross section of only $120\,\mathrm{mm}^2$ compared to $227\,\mathrm{mm}^2$ on the existing design. These were Guangdong Kingly Gear Co. Micro Metal Gearmotors (50:1) [26], were lighter than the existing motors, 18 g compared to 27 g, and the mechanism would be less complex. These motors have a much lower $\theta_{\max}$ than the existing motors of only $44\,\mathrm{rad\,s^{-1}}$ compared to $442\,\mathrm{rad\,s^{-1}}$ [27], but since the original experiments limited the motor velocity to $10\,\mathrm{rad\,s^{-1}}$ to ensure mechanism stability, this is not a concern. This change of motors allowed r to be reduced from 13 mm to 7.25 mm.

TABLE I: Table of the minimum and maximum values of $\Lambda(\boldsymbol{\theta})$ at different values of r in the interval of $\left[-\frac{\pi}{2}, \frac{\pi}{2}\right]$.

r [mm]	$\lambda_1(\boldsymbol{\theta})$ [mm]		$\lambda_2(\boldsymbol{\theta})$ [mm]		$\lambda_3(\boldsymbol{\theta})$ [mm]	
	Min.	Max.	Min.	Max.	Min.	Max.
13.0	42.64	68.35	42.64	68.57	42.64	68.57
10.0	45.02	64.88	45.02	64.98	45.02	64.98
7.25	47.33	61.78	47.33	61.82	47.33	61.82

In order to facilitate this reduction, other alterations to the design were required. The distance between the TSA strings was now too small to have a central shaft in the middle, as was the case in the original design. Instead of having a central shaft for the universal joint, the universal joint was constructed around the TSA with a "hollow spider" arrangement, where the TSA strings pass through a hole in the middle of the universal joint, as illustrated in figure 3. This also meant there was enough space to allow the installation of AUJ angle sensors directly onto the universal joint, which are discussed in section II-B.

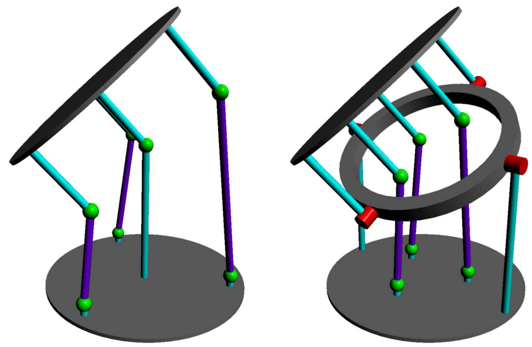

Fig. 3: An AUJ with a central universal joint, and one with a hollow spider. The hollow spider allows r to be decreased as space is no longer required for a central universal joint.

B. Improving AUJ Angle Measurement Accuracy

The original design used a Bosch Sensortec BNO080 9 DOF inertial measurement unit (IMU) [28] to measure the AUJ orientation. The original plan was to use two IMUs, on the base and follower bodies, and the orientation would be calculated from the difference. However, the magnetometer measurements proved to be unreliable inside the laboratory, so only a single IMU was used and the base segment was orientated with the gravity vector parallel to the z axis. due to inconsistent magnetometer readings inside the laboratory, only one IMU was implemented, aligning the base body with gravity along the z axis. This allowed the AUJ orientation to be calculated from only the accelerometer readings, but meant the mechanism could only be controlled when orientated in the vertical axis.

There was also an issue with the IMU resolution, which was only accurate to within $\pm 1.5°$ [28]. A Savitsky-Golay filter was applied to the results in [23] for data presentation purposes and to more accurately represent the true AUJ angles at that point in time.

To enable the mechanism to be controlled in any direction relative to gravity, a solution that can directly measure the mechanical angular displacement of the universal joint was required. Two options were considered, potentiometers and hall effect sensors. A potentiometer would couple a shaft of each universal joint spider axes to a resistive track, changing its resistance depending on AUJ orientation and providing an analog voltage signal to the controller. A hall effect sensor would be similar to the potentiometer solution, but would use a radially bipolar magnet on the end of the shaft with a hall effect sensor beneath it, which would also provide an analog voltage signal or digital data for the axial orientation of the magnet, and therefore the shaft [29]. The potentiometer solution was chosen due to simplicity of control integration and integrated mechanical stops, which guarantee the required AUJ angle range will able be measured during assembly. The hall effect sensor is continuous, and the measured voltage overflows every 180° [29], so it would be very important to ensure the magnet was initially oriented at a value that would encompass both the maximum and minimum joint limit for each AUJ axis. The Bourns PDB08 was selected as the potentiometer due to its small size and internally threaded shaft, which would allow a captive bolt to be inserted as the spider shaft [30]. As a voltage divider at $+5\,\mathrm{V}$, the PDB08 would have a resolution of approximately $40\,°\,\mathrm{V}^{-1}$. With the 12-bit resolution of the onboard analog to digital converter (ADC) for myRIO analog inputs, this gives a theoretical resolution of $\approx 0.048°$. The potentiometer sliding noise (max. $100\,\mathrm{mV}$) will reduce this during AUJ motion, however this can be partially mitigated with filtering.

C. Preventing String Failure

One reoccurring issue with the original experiments were the TSA strings breaking at high values of θ_s, which became more common after a number of twisting and untwisting cycles. Occasionally this was caused by the mechanism operating beyond expected limits for θ_s and f due to a failure of limit monitoring within the control system, but failure would also occur within normal operating conditions.

Analysis of the design and the location of the string failures identified “pinch points”, where the string was “pinched“ between two surfaces, which could deform the string and weaken it, and “bite points”, where the string rested over a sharp edge, which could “bite” into the string and weaken it if pushed into the edge, as shown in figure 4a.By removing these points, by rounding off sharp edges and using an alternative method to secure the string, tying it into a loop instead of using grub screws, eliminated these potential sources of string damage, as shown in figure 4b. However, nylon monofilament, as was used for the TSA string, is still susceptible to torsion fatigue [31], [32] which reduces tensile strength [33]. This means the monofilament string will be increasingly susceptible to failure with more twisting and untwisting cycles. Therefore, the SeaKnight BLADE 0.2 mm nylon monofilament was exchanged for 0.2 mm Dyneema® polyfilament string, as used in [12]. Changes to the design of the string clamp allowed for easier installation of string filament, making polyfilament string a practical option.

D. Final Improved Design

Figure 5 shows an annotated schematic of the improved design. The load cells were kept the same as the original design, and the universal joints below the load cells were altered. The hollow spider was connected to the base and follower bodies with machine precision bearings and bushings to allow for smooth motion. The control system remained broadly the same as the original design, except the Faulhaber MCDC3002 motor controllers [34] were exchanged for a single Pimoroni Motor 2040 which could handle up to four Micro Metal Gearmotors with Micro Metal Motor Encoders attached. This was programmed with a velocity controller similar to the example given in the `pimoroni-pico` library. The deadband compensation threshold was also reduced to $\pm 0.5\,\mathrm{rad\,s^{-1}}$ as the motors

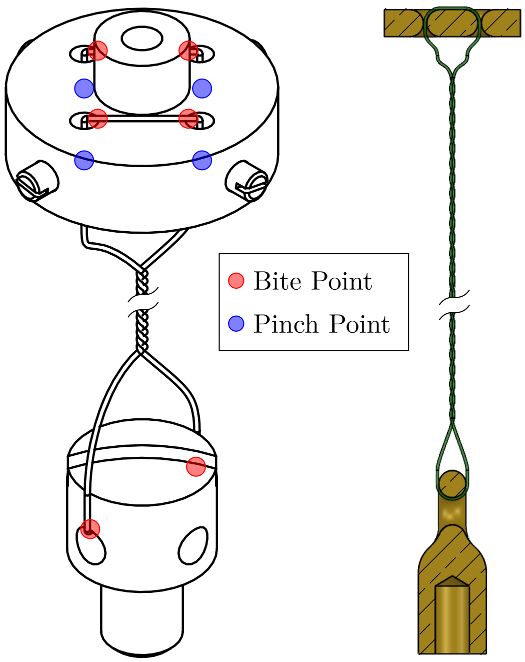

(a) (b)

Fig. 4: (a) The original TSA string loop between the string clamp and capstan bolt, with “pinch” and “bite” points indicated, where premature string failure may occur. (b) Section view of the new TSA string loop showing how there pinch and bite points have been eliminated.

TABLE III: PID gains used for the experiment.

Gain	Value	
	Windup	Tracking
k_p	2×10^5	8×10^5
k_i	3500	3500
k_d	0	50
k_{p_s}	5	5

had a much smaller deadband region, but the motor velocity limit of $10\,\mathrm{rad\,s^{-1}}$ remained the same.

TABLE II: Model coefficients for the improved design.

Coeff.	Value		Coeff.	Value	
l_1	55	mm	f_{min}	3	N
l_2	0	mm	r_s	200	µm
r	7.25	mm	m	61.6	g
l_u	55	mm	$\dot{\theta}_{s_{\max}}$	44	$\mathrm{rad\,s^{-1}}$
$\tau_{\max}$	0.039	N m	$\boldsymbol{\rho}$	$\begin{bmatrix}0 & 0 & 3.05\end{bmatrix}$	mm
Coeff.	**Value**				
I	$\begin{bmatrix}2.8 \times 10^{-5} & 0 & 0 \\ 0 & 2.6 \times 10^{-5} & 0 \\ 0 & 0 & 5 \times 10^{-6}\end{bmatrix}$	$\mathrm{kg\,m^{-2}}$			

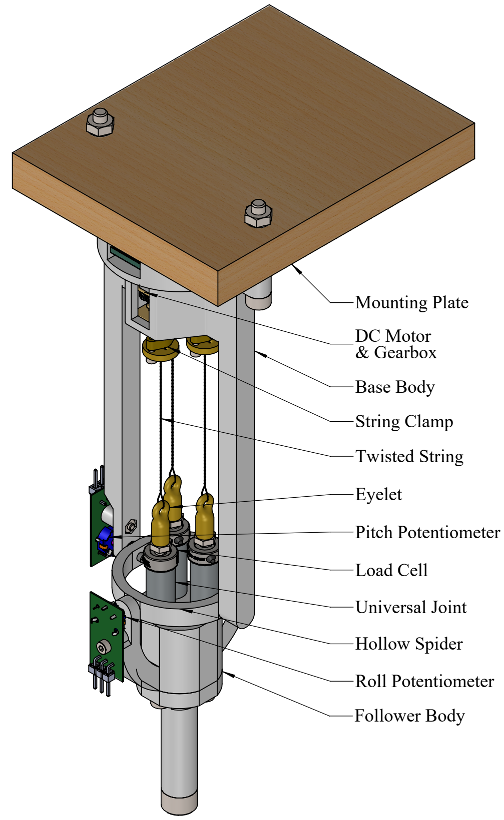

Fig. 5: Schematic of the improved design with labelled components.

III. Experimental Results

A. AUJ Angle Tracking

Figure 6 plots the tracking response of the experiment in the pitch and roll axis. Three trajectories were created to test the capabilities of the mechanism. Two were only in one axis of the AUJ, and the third was in both axes. The angle range of the AUJ was limited to $\pm 26°$ due to mechanical limitations, namely the hollow spider colliding with the TSA universal joints in the pitch axis and the follower body in the roll axis. The angle range was also limited to $\pm 20°$ for the dual axis trajectory, or the trajectory would be aborted prematurely, due to a load cell exceeding a safety limit of 9 N (the load cell full scale is 9.8 N [35]).

B. The Effect of Follower Mass on AUJ Angle Tracking

If a multi-segment design is to be realised, the performance of the AUJ with a non-negligible follower mass must be analysed. This is because adding mass to the follower body changes the dynamics of the system as shown in table IV, which affects the inverse dynamic calculations in the control system. Figure 7 shows the response for a roll trajectory with different amounts of mass added to the follower body, namely 20 g, 50 g and 80 g. Larger masses

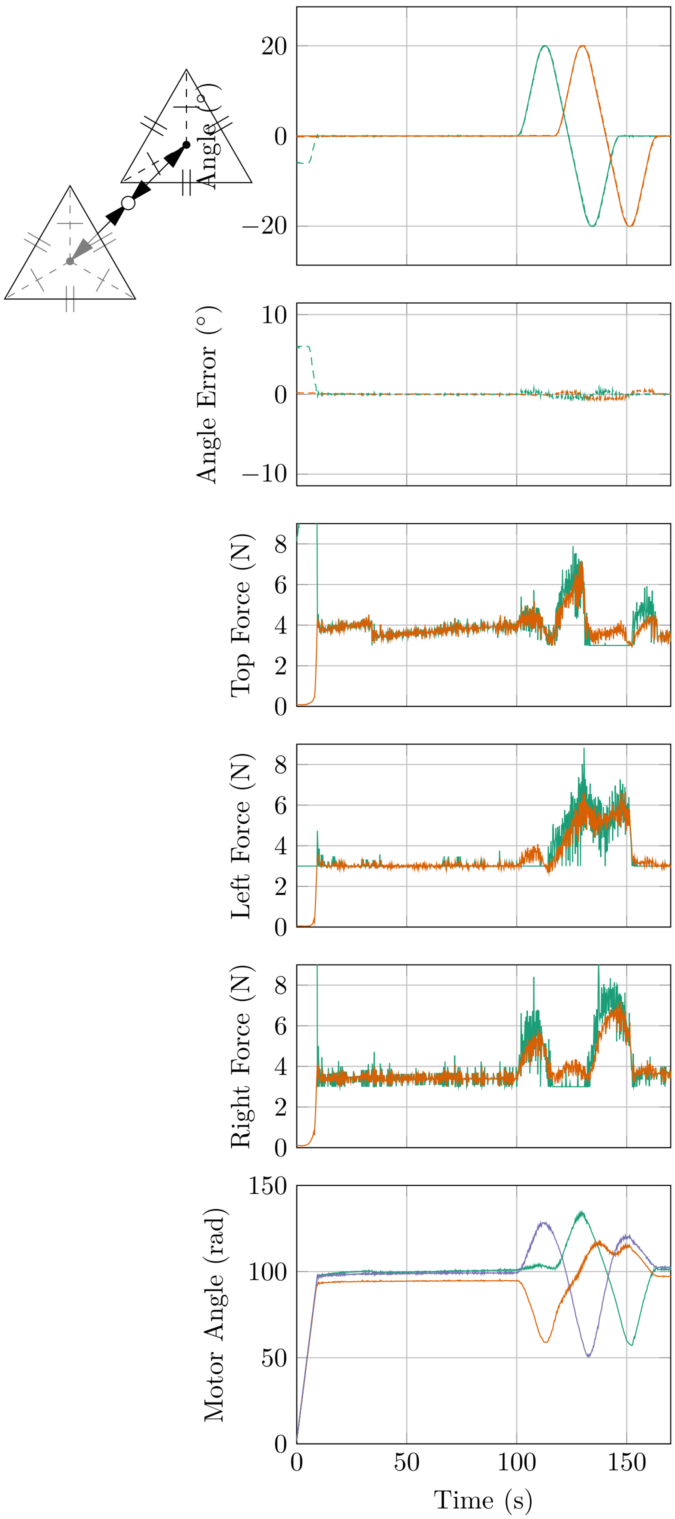

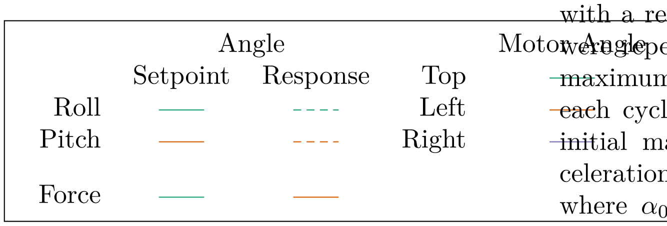

Fig. 6: Plots of the response for both axes θ_1 and θ_2. Plots include AUJ orientation, forces at the top, left and right TSA, and the motor positions.

TABLE IV: Table of all the follower mass configurations, with the parameters for follower mass m and follower COM z offset ρ_3.

Config.	m [g]	ρ_3 [mm]	I [kg m^{-2}]	Image
No Mass	62	3.1	$\mathrm{diag}\left(\begin{bmatrix}2.8\times10^{-5}\\2.6\times10^{-5}\\5.0\times10^{-6}\end{bmatrix}^\intercal\right)$	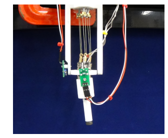
+20.0 g	160	35	$\mathrm{diag}\left(\begin{bmatrix}6.9\times10^{-5}\\6.8\times10^{-5}\\7.0\times10^{-6}\end{bmatrix}^\intercal\right)$	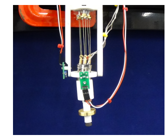
+50.0 g	260	43	$\mathrm{diag}\left(\begin{bmatrix}1.1\times10^{-4}\\1.1\times10^{-4}\\1.1\times10^{-5}\end{bmatrix}^\intercal\right)$	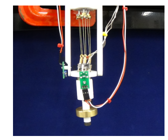
+80.0 g	360	46	$\mathrm{diag}\left(\begin{bmatrix}1.3\times10^{-4}\\1.3\times10^{-4}\\1.2\times10^{-5}\end{bmatrix}^\intercal\right)$	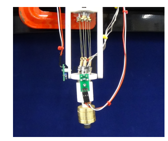

could not be used as the trajectory would be aborted prematurely, due to a load cell exceeding a safety limit of 9 N. Initially, k_p was set to the same value as in table II, however the system was unable to reach a steady state in any configuration other than “No Mass”. Reducing k_p to 1000 in the weighted configurations solved the steady state issue and resulted in an average maximum tracking error of 0° over all configurations with added mass, similar to the result from the initial experiments. However, for the “No Mass” configuration, $k_p = 8000$ resulted in a very poor tracking response, whereas k_p from table II resulted in a maximum tracking error of 0°, once again similar to the result from the initial experiments. In future implementations gain scheduling can be employed to select the most optimal k_p for a given follower mass, that allows for the smallest tracking error while being able to reach a steady state.

C. The Effect of AUJ Angular Velocity on AUJ Angle Tracking

To verify the performance of the AUJ at higher angular velocities, the single axis experiments from section III-A, with a reduced angle range of ±23° in case of overshoot, were repeated with a trapezoidal “chirp” signal, with the maximum angular velocity increasing by $\omega_0 + (2\,(n-1)\,\omega_0)$ each cycle, where n is the cycle number, and w_0 is the initial maximum angular velocity, and the angular acceleration increasing by $\alpha_0 + (16\,(n-1)\,\alpha_0)$ each cycle, where α_0 is the initial angular acceleration. A total of four cycles were performed, with the maximum velocity and acceleration values shown in table V. Figure 8 shows the results of these experiments, which shows the tracking

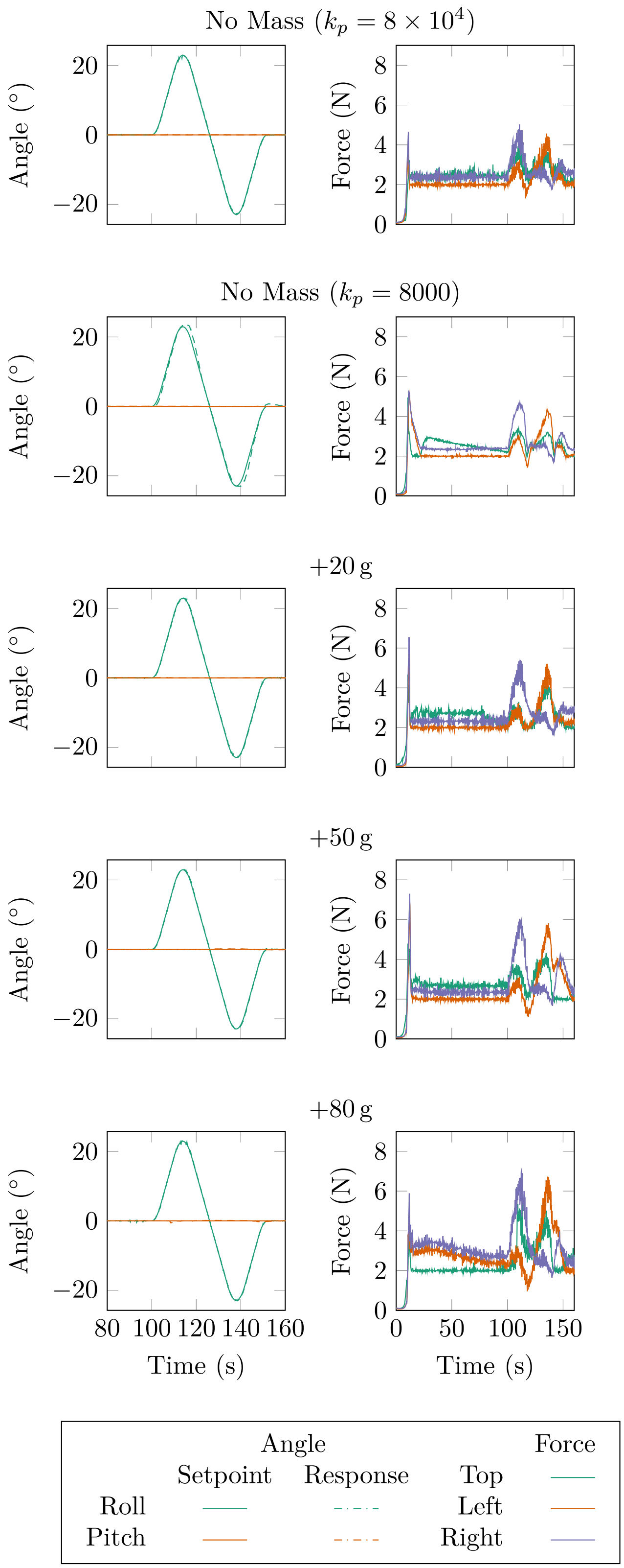

Fig. 7: AUJ roll tracking with increasing follower mass from table IV, plus with no mass at $k_p = 8000$ and $k_p = 8 \times 10^4$.

TABLE V: Trapezoidal trajectory sequence parameters.

Cycle	Max./Min. Angle [rad]	Max. Velocity [rad s^{-1}]	Acceleration [rad s^{-2}]
1	0.4	0.4	0.01
2	0.4	0.44	0.011
3	0.4	0.484	0.0121
4	0.4	0.5324	0.013 31

error increasing marginally as maximum angular velocity and acceleration increases. The pitch experiment was unable to be completed as the maximum load cell force went above the safety limit of 9 N, as can be seen in the figure.

IV. Discussion

A. Active Transmission Adjustment (ATA)

One notable property of the TSA mechanism is the non-linear transmission ratio that is dependant on θ_s, as shown in figure 9. This means that the performance characteristics of the TSA, specifically the maximum stroke velocity $\dot{p}_{\max}$ and maximum tensile force $f_{\max}$. These characteristics have an inverse relationship as θ_s increases, with $f_{\max}$ decreasing and $\dot{p}_{\max}$ increasing.

Using the jacobian from [14], $f_{\max}$ and $\dot{p}_{\max}$ are found as

$$\begin{aligned} \mathcal{J} &= \frac{\theta_s r_s^2}{l_u - p} \\ \mathcal{J}^{-1} &= \frac{l_u - p}{\theta_s r_s^2} \\ f_{\max} &= \mathcal{J}^{-1}\tau_{\max} \\ \dot{p}_{\max} &= \mathcal{J}\dot{\theta}_{s_{\max}}. \end{aligned} \tag{4}$$

Therefore, for the same stroke p, increasing θ_s will decrease $f_{\max}$ and increase $\dot{p}_{\max}$. The effect is even greater if p increases.

In order to change $f_{\min}$, the minimum value of θ_s has to be increased for each TSA, since $\boldsymbol{f}$ will always be the same value when the TSA are fully unwound ($p = 0$). This means that by changing $f_{\min}$, the performance of the TSA, and therefore AUJ, can be altered in real time during operation. The maximum AUJ joint velocity can be reduced in favour or increased maximum AUJ joint torque, or vice versa. This has applications where performance characteristics need to be altered temporarily to perform a specific action, such as a mobile snake robot lifting up segments off the ground, or a prosthesis that needs to be ready to perform a faster motion while unencumbered. By reducing r, the stroke length is significantly smaller as shown in table I, so f_{min} could be adjusted within a much larger interval compared to the original design.

It may be noticed that $\lim_{\theta_s \to 0} f_{\max} = \infty$. This is due to the assumption of an infinite material stiffness for the strings, which would not be possible outside simulation and is a significant issue for high force applications as detailed in [14].

Experiments were conducted to try and verify this concept by executing the same AUJ trajectory with increasing

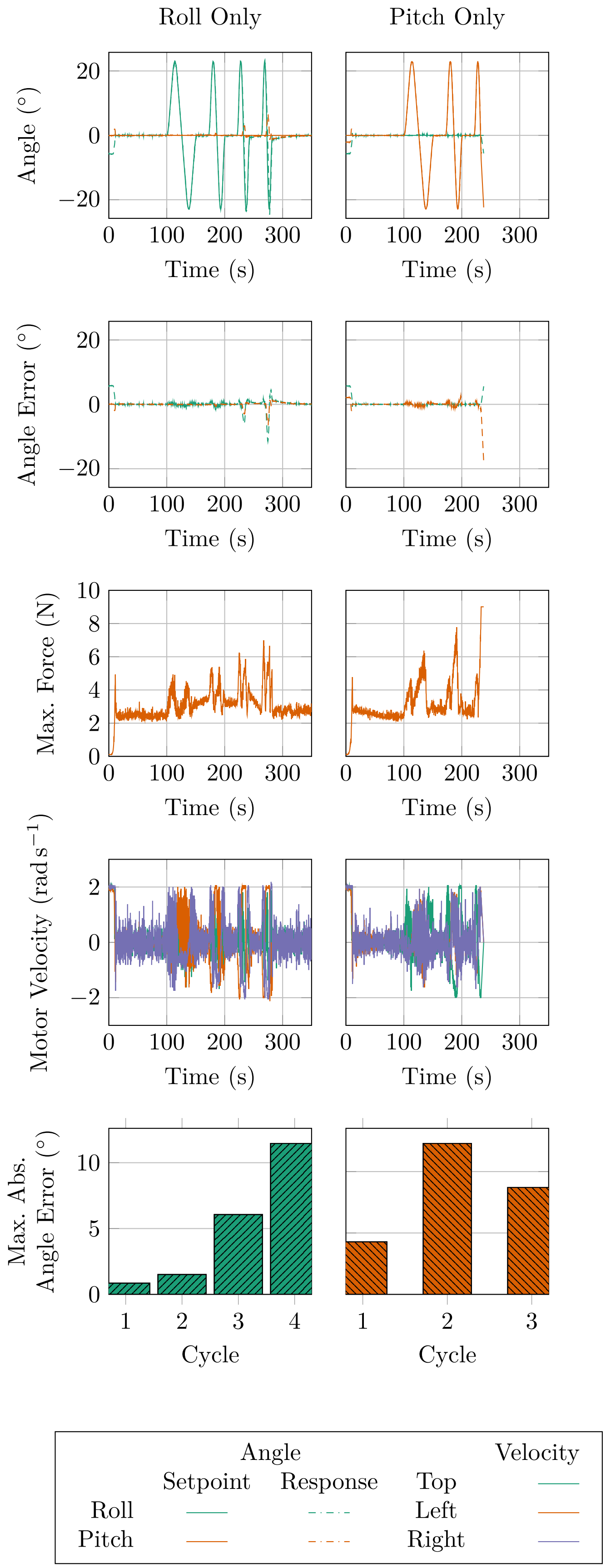

Fig. 8: Results of the trapezoidal velocity trajectory from table V for both AUJ pitch and roll trajectories, including the maximum absolute angle error for each cycle.

values of f_{min}. By measuring the current consumption of all of the motors, it was hoped at an increase in current consumption would be noticed as f_{min}, and therefore the minimum value of θ_s, increased. This is because the motor torque required to maintain an increasing θ_s also increases if stroke p remains constant [14], which would be the case for the same AUJ angle position for different values of f_{min}, as shown by (2). However, due to the properties of the low cost brushed DC motors, such as backlash in the gearbox, and the nature of PWM control, it was not possible to determine this relationship. Future work would include better analysis methods, or possibly changing the motors for brushless DC motors, to see if this relationship can be verified experimentally.

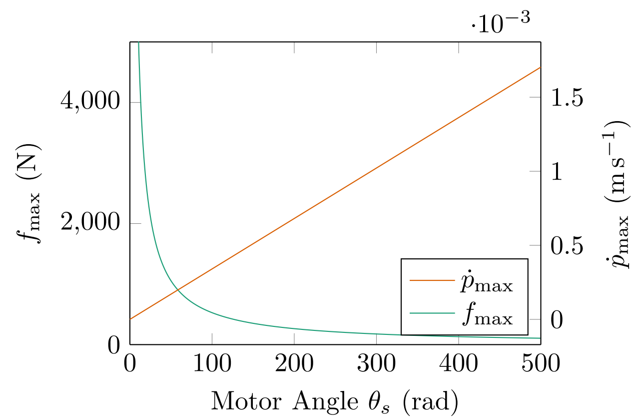

Fig. 9: By adjusting f_{min}, the transmission ratio of the TSA can be altered. Reducing f_{min} increases the maximum TSA force f_{max} while reducing the maximum TSA stroke velocity $\dot{p}_{\text{max}}$. Conversely, increasing f_{min} reduces f_{max} and increases $\dot{p}_{\text{max}}$. This can be used to actively modify the dynamic properties of the AUJ during operation. In this graph, $p = 0$.

B. *Dynamics Gravity Vector*

In the experiments, the gravity vector $\boldsymbol{g}$ was assumed to be parallel to the z axis ($\begin{bmatrix} 0 & 0 & -9.81 \end{bmatrix}$) since the experiments were conducted in a vertical orientation. To operate in any other orientation, the gravity vector would need to be calculated using an IMU (gyroscopes would be required to compensate for forces generated using motion).

C. *Load Cell Limitation*

As noted in sections III-A, III-B and III-C, the load on each TSA being limited to 9 N meant that the AUJ angle range was limited with an increased follower mass, increased velocity, and in dual axis operation. Using load cells with a larger full scale would increase the AUJ angle range in all cases.

D. *Multi-Segment Design*

For a multi-segment system, a distributed embedded control system in each segment could receive AUJ angle position setpoint commands from a "primary" controller. This would allow for complex trajectories to be executed while allowing the segments to share a common power and communication bus, reducing wiring complexity and allowing for a modular design.

V. Conclusion

This research has documented various improvements made to an existing design for an actuated universal joint using twisted string actuator, and successfully demonstrated the improvement in AUJ angle range, increasing from $\pm 14.5°$ to $\pm 26°$, string reliability, and AUJ angle measurement accuracy. It has also investigated the possibility of active transmission adjustment, which would allow for performance characteristics to be altered during operation, which has potential applications in robotics and prosthetics. Additional experiments characterising the velocity and follower load performance of the system have also been carried out. Finally, remaining limitations have been discussed and solutions proposed, as well as a discussion on the requirements and a potential control framework for a multi-segment system has been outlined.

VI. Acknowledgement

This work was supported by a UKRI EPSRC Doctoral Training Partnership [1957210], and by the UKRI Strength in Place Fund [84646 (AMPI)]. The lead author also wishes to thank Dr. Dmitriy Makhnovskiy for his assistance in preliminary research for this publication.

References

[1] R. Buckingham and A. Graham, "Nuclear snake-arm robots," *Industrial Robot: An International Journal*, 2012.

[2] M. Luo, R. Yan, Z. Wan, *et al.*, "Orisnake: Design, fabrication, and experimental analysis of a 3-d origami snake robot," *IEEE Robotics and Automation Letters*, vol. 3, no. 3, pp. 1993–1999, 2018.

[3] W. S. Rone, W. Saab, and P. Ben-Tzvi, "Design, Modeling, and Integration of a Flexible Universal Spatial Robotic Tail," *Journal of Mechanisms and Robotics*, vol. 10, no. 4, Apr. 2018, 041001, ISSN: 1942-4302. DOI: 10.1115/1.4039500.

[4] A. Rezaei, Y. Shekofteh, M. Kamrani, A. Fallah, and F. Barazandeh, "Design and control of a snake robot according to snake anatomy," in *2008 International Conference on Computer and Communication Engineering*, IEEE, 2008, pp. 191–194.

[5] T. Baba, Y. Kameyama, T. Kamegawa, and A. Gofuku, "A snake robot propelling inside of a pipe with helical rolling motion," in *Proceedings of SICE Annual Conference 2010*, IEEE, 2010, pp. 2319–2325.

[6] C. Wright, A. Buchan, B. Brown, *et al.*, "Design and architecture of the unified modular snake robot," in *2012 IEEE international conference on robotics and automation*, IEEE, 2012, pp. 4347–4354.

[7] G. Qin, Y. Cheng, A. Ji, *et al.*, "Research on the cable-driven endoscopic manipulator for fusion reactors," *Nuclear Engineering and Technology*, 2023.

[8] T. Würtz, C. May, B. Holz, C. Natale, G. Palli, and C. Melchiorri, "The twisted string actuation system: Modeling and control," in *2010 IEEE/ASME International Conference on Advanced Intelligent Mechatronics*, Jul. 2010, pp. 1215–1220. DOI: 10.1109/AIM.2010.5695720.

[9] P. Muehlbauer, M. Schimbera, K. Stewart, and P. P. Pott, "Twisted string actuation for an active modular hand orthosis," in *ACTUATOR; International Conference and Exhibition on New Actuator Systems and Applications 2021*, VDE, 2021, pp. 1–4.

[10] J. Park, J.-i. Park, H.-T. Seo, Y. Liu, K.-S. Kim, and S. Kim, "Control of tendon-driven (twisted-string actuator) robotic joint with adaptive variable-radius pulley," in *2020 20th International Conference on Control, Automation and Systems (ICCAS)*, IEEE, 2020, pp. 1096–1098.

[11] B. Suthar and S. Jung, "Design and feasibility analysis of a foldable robot arm for drones using a twisted string actuator: Frad-tsa," *IEEE Robotics and Automation Letters*, vol. 6, no. 3, pp. 5769–5775, 2021. DOI: 10.1109/LRA.2021.3084890.

[12] G. Palli, C. Natale, C. May, C. Melchiorri, and T. Wurtz, "Modeling and control of the twisted string actuation system," *IEEE/ASME Transactions on Mechatronics*, vol. 18, no. 2, pp. 664–673, 2012.

[13] R. Budynas and J. Nisbett, *Shigley's Mechanical Engineering Design* (McGraw-Hill series in mechanical engineering). McGraw-Hill, 2011, pp. 416–417, ISBN: 9780071328401.

[14] S. Nedelchev, I. Gaponov, and J. Ryu, "Accurate dynamic modeling of twisted string actuators accounting for string compliance and friction," *IEEE Robotics and Automation Letters*, vol. 5, no. 2, pp. 3438–3443, 2020. DOI: 10.1109/LRA.2020.2970651.

[15] S. Nedelchev, I. Gaponov, and J.-H. Ryu, "Design of robotic gripper with constant transmission ratio based on twisted string actuator: Concept and evaluation," in *2018 IEEE/RSJ International Conference on Intelligent Robots and Systems (IROS)*, IEEE, 2018, pp. 967–972.

[16] M. F. Rahman, K. Zhang, and G. Herrmann, "Modular, underactuated anthropomorphic robot hand with flexible fingers and twisted string actuators," in *Towards Autonomous Robotic Systems: 20th Annual Conference, TAROS 2019, London, UK, July 3–5, 2019, Proceedings, Part II 20*, Springer, 2019, pp. 489–492.

[17] V. Skvortsova, S. Nedelchev, J. Brown, I. Farkhatdinov, and I. Gaponov, "Design, characterisation and validation of a haptic interface based on twisted string actuation," *Frontiers in Robotics and AI*, vol. 9, p. 977 367, 2022.

[18] M. Usman, B. Suthar, H. Seong, E. Hawkes, I. Gaponov, and J.-H. Ryu, “Passive returning mechanism for twisted string actuators,” in *2017 IEEE International Conference on Robotics and Automation (ICRA)*, IEEE, 2017, pp. 3714–3719.

[19] D. Popov, I. Gaponov, and J.-H. Ryu, “Bidirectional elbow exoskeleton based on twisted-string actuators,” in *2013 IEEE/RSJ International Conference on Intelligent Robots and Systems*, IEEE, 2013, pp. 5853–5858.

[20] J. Park, J. H. Kim, K.-S. Kim, and S. Kim, “Design and control of antagonistic robot joint with twisted string actuators,” in *2016 13th International Conference on Ubiquitous Robots and Ambient Intelligence (URAI)*, IEEE, 2016, pp. 563–565.

[21] D. Lee, D. H. Kim, C. H. Che, J. B. In, and D. Shin, “Highly durable bidirectional joint with twisted string actuators and variable radius pulley,” *IEEE/ASME Transactions on Mechatronics*, vol. 25, no. 1, pp. 360–370, 2019.

[22] R. Konda, D. Bombara, E. Chow, and J. Zhang, “Kinematic modeling and open-loop control of a twisted string actuator-driven soft robotic manipulator,” *Journal of Mechanisms and Robotics*, pp. 1–18, 2023.

[23] D. Crosby, J. Carrasco, W. Heath, and A. Weightman, “A novel triad twisted string actuator for controlling a two degrees of freedom joint: Design and experimental validation,” in *2022 International Conference on Robotics and Automation (ICRA)*, IEEE, 2022, pp. 11 388–11 394.

[24] F. Dessen, “Coordinating control of a two degrees of freedom universal joint structure driven by three servos,” in *Proceedings. 1986 IEEE International Conference on Robotics and Automation*, vol. 3, Apr. 1986, pp. 817–822. DOI: 10.1109/ROBOT.1986.1087559.

[25] M. W. Spong, S. Hutchinson, and M. Vidyasagar, *Robot modeling and control*. John Wiley & Sons, 2020.

[26] *Jl-12fn20-50-06420*, Guangdong Kingly Gear Co.

[27] *Dc micromotors - precious metal commutation*, Dr. Fritz Fauhaber GmbH & Co. KG, Feb. 2020.

[28] *Bno080 data sheet*, 1.3, Hillcrest Laboratories, Inc., Oct. 2017.

[29] K. Bienczyk, “Angle measurement using a miniature hall effect position sensor,” in *2009 2nd International Students Conference on Electrodynamic and Mechatronics*, IEEE, 2009, pp. 21–22.

[30] *Pdb08 - 8 mm micro rotary potentiometer*, Bourns, Mar. 2021.

[31] B. Goswami and J. Hearle, “A comparative study of nylon fiber fracture,” *Textile Research Journal*, vol. 46, no. 1, pp. 55–70, 1976.

[32] M. Toney and P. Schwartz, “Bending and torsional fatigue of nylon 66 monofilaments,” *Journal of applied polymer science*, vol. 46, no. 11, pp. 2023–2032, 1992.

[33] D. Hennessey, E Carey, C. Simms, A Hanly, and D. Winter, “Torsion of monofilament and polyfilament sutures under tension decreases suture strength and increases risk of suture fracture,” *Journal of the Mechanical Behavior of Biomedical Materials*, vol. 12, pp. 168–173, 2012.

[34] *Motion controllers - series mcdc 3002 s*, 6th ed., Dr. Fritz Fauhaber GmbH & Co. KG, Nov. 2018.

[35] *Lcm100 miniature in line load cell*, FUTEK Advanced Sensor Technology Inc.

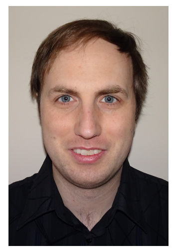

Dr. Damian J. Crosby is a Post Doctoral Research Associate in the Department of Mechanical, Aerospace and Civil Engineering, University of Manchester, U.K. He received a B.Sc. in Special Effects Development from The University of Bolton, U.K., in 2010, and a M.Res. in Robotics from The University of Plymouth, U.K., in 2012. He worked as a Research Technician in robotic laser welding at The University of Manchester from 2013 to 2017, and then completed his PhD at the same university in 2023, developing a robotic tail for improved robot balance when carrying a payload. He has worked on robotic research in the fields of nuclear energy and advanced manufacturing.

Dr. Joaquin Carrasco is a Lecturer at the Department of Electrical and Electronic Engineering, University of Manchester, UK. He was born in Abarn, Spain, in 1978. He received the B.Sc. degree in physics and the Ph.D. degree in control engineering from the University of Murcia, Murcia, Spain, in 2004 and 2009, respectively. From 2009 to 2010, he was with the Institute of Measurement and Automatic Control, Leibniz Universitt Hannover, Hannover, Germany. From 2010 to 2011, he was a Research Associate at the Control Systems Centre, School of Electrical and Electronic Engineering, University of Manchester, UK.

Prof. William P. Heath is Chair of Feedback and Control in the Department of Electrical and Electronic Engineering, University of Manchester, U.K. He received the B.A. and M.A. degrees in mathematics from Cambridge University, U.K., in 1987 and 1991, and the M.Sc. and Ph.D. degrees in systems and control from the University of Manchester Institute of Science and Technology, U.K., in 1989 and 1992, respectively. He was with Lucas Automotive from 1995 to 1998 and was a Research Academic at the University of Newcastle, Australia from 1998 to 2004. His research interests include absolute stability, multiplier theory, constrained control, and system identification.

Prof. Andrew Weightman graduated in 2006 with a PhD in Mechanical Engineering form the University of Leeds. Whilst at the University of Leeds he developed rehabilitation robotic technology for improving upper limb function in adults and children with neurological impairment which was successfully utilised in homes, schools and clinical settings. In 2013 he moved to the University of Manchester, Department of Mechanical, Aerospace and Civil Engineering as a Lecturer in Medical Mechatronics. Prof. Weightman has research interests in biomimetic mobile robotics, rehabilitation robotics, robotics for nuclear decommissioning and collaborative robotics.